Energy Conversion and Management 276 (2023) 116480

Contents lists available at ScienceDirect

Energy Conversion and Management

journal homepage: www.elsevier.com/locate/enconman

Process analysis for the simultaneous production of aromatics and syngas from shale gas and CO_2

Wonho Jung [a], Hyeona Kim [a], Hae Won Ryu [b], Yong Hyun Lim [b], Do Heui Kim [b,*], Jinwon Lee [a,c,*]

[a] C1 Gas Refinery R&D Center, Sogang University, 35 Baekbeom-ro, Mapo-gu, Seoul 04107, Republic of Korea
[b] School of Chemical and Biological Engineering, and Institute of Chemical Processes, Seoul National University, 1 Gwanak-ro, Gwanak-gu, Seoul 08826, Republic of Korea
[c] Department of Chemical and Biomolecular Engineering, Sogang University, 35 Baekbeom-ro, Mapo-gu, Seoul 04107, Republic of Korea

ARTICLE INFO

Keywords:
BTX production from shale gas
Non-oxidative reaction
CO_2 co-feeding reaction
Surrogate model based optimization
Technoeconomic analysis
Life cycle assessment

ABSTRACT

The production of benzene, toluene, and xylene (BTX) from shale-derived CH_4, C_2H_6, and C_3H_8 is considered a promising alternative to their fossil-based counterparts. Herein, we evaluate a production technology for aromatics and hydrogen with non-oxidative and CO_2 co-feeding reactions to predict the economics and environmental impact of each process. The optimal process for producing aromatics and hydrogen varies depending on the presence or absence of CO_2, and we experimentally confirm the difference in the reaction systems. The operating conditions of both processes are optimized using an experiment-based surrogate model in terms of thermal energy demand and profit of products, which account for the highest portion of BTX production cost. Particularly, the CO_2 emissions and economic feasibility of the proposed BTX production processes are compared with those of an ethane cracking center using shale gas and the naphtha reforming/Cyclar process to produce BTX. In the CO_2 co-feeding case, the CO_2 reduction effect is proven compared to other processes, and the economics was improved by the sale of H_2 and CO compared to the non-oxidative BTX production. Furthermore, the BTX production cost reflecting the carbon price is comparable to that of commercial processes; as the carbon price increases, the economics has the potential to outperform existing processes. These findings present a platform for economic evaluation based on CO_2 emissions as well as the economic benefits of processes that reduce CO_2 emissions for energy-efficient conversion of shale gas into high value-added products.

1. Introduction

The production of benzene, toluene, and xylene (BTX) via the co-aromatization of shale gas, including CH_4, C_2H_6, and C_3H_8 is a promising alternative for producing high-value-added chemicals from shale gas [1–3]. In our previous studies, an economic evaluation was performed by linking the shale gas-based BTX production and the subsequent CH_4 utilization processes, and the effect of reducing CO_2 was discussed [4]. Furthermore, CO_2 co-feeding BTX production over Mo/HZSM-5 prevented carbon deposition on the catalyst [5,6], resulting in a more stable process to dehydroaromatize hydrocarbons (HCs). Co-feeding CO_2 in BTX production increases the H_2 production rate by the dry reforming of HCs in shale gas and positively affects the process economics and environmental impact [7]. However, to improve the competitiveness of BTX production technology, economic benefits should be maximized by considering only BTX production without a subsequent CH_4 utilization process.

Among the processes using shale gas, the most representative is the ethane cracking center (ECC) [8]. CH_4, which is a major component of shale gas, is separated from C_2H_6 and C_3H_8 by cryogenic distillation and is mainly used to produce electricity, whereas C_2H_6 and C_3H_8 are used to produce C_2H_4 and C_3H_6 by steam cracking reaction [9–11]. The ECC accounts for approximately 55 % of ethylene production in the USA and is regarded as the most efficient commercial process for shale gas [12]. The non-catalytic steam-cracking reaction of ECC process has a high carbon yield of 70–80 % [13] and thus exhibits high economic benefits.

* Corresponding authors at: School of Chemical and Biological Engineering, and Institute of Chemical Processes, Seoul National University, 1 Gwanak-ro, Gwanak-gu, Seoul 08826, Republic of Korea (D.H. Kim), Department of Chemical and Biomolecular Engineering, Sogang University, 35 Baekbeom-ro, Mapo-gu, Seoul 04107, Republic of Korea (J. Lee).
E-mail addresses: dohkim@snu.ac.kr (D.H. Kim), jinwonlee@sogang.ac.kr (J. Lee).

https://doi.org/10.1016/j.enconman.2022.116480
Received 14 September 2022; Received in revised form 31 October 2022; Accepted 10 November 2022
Available online 24 November 2022

Commercial processes for producing BTX include the traditional naphtha reforming process and the Cyclar process using light HCs (C_3H_8 or C_4H_{10}). Naphtha reforming accounts for approximately 54 % of global BTX production, and Pt-based Al_2O_3 catalyst is mainly used [14]. The BTX yield is approximately 60 %, which sufficiently guarantees the economic feasibility. In the Cyclar process [15], the feed source may include C_3H_8/C_4H_{10} mixtures; the BTX yield is ~ 60 %. Ga-based zeolite catalysts are mainly used in this process [16], and the process scheme is not significantly different from that of naphtha reforming. In the proposed BTX production process from shale gas, the BTX yield is considerably low (approximately 10 %) in the general shale gas composition [4]. However, compared with ECC, aromatics and additional by-product H_2 are produced; this provides a different approach to using shale gas. Moreover, in contrast to other BTX processes, the economic efficiency can be improved by utilizing unreacted CH_4 and linking it with subsequent processes. Therefore, the CO_2 emissions and economic feasibility of the BTX production process from shale gas should be comprehensively compared with those of the aforementioned processes.

When producing BTX from shale gas, various intermediates or by-products are produced, which are highly dependent on temperature and feed composition. Experimentally verifying these variables is labor-intensive and time-consuming [17]. Consequently, several optimization methods have been developed based on surrogate models [18]. A surrogate model can effectively represent the target model and facilitate efficient model analyses and optimization [19]. A surrogate model can be regarded as a "regression" to a set of data, where the data are sets of input–output pairings obtained by evaluating a black-box model of the complex system. Yan and coworkers proposed a Bayesian migration methodology for Gaussian process regression (GPR) to promote rapid process modeling and optimization [20]. GPR-based modeling can effectively describe both practical chemical and simulated processes. In the Bayesian optimization algorithm, the objective function is evaluated sequentially and iteratively using a stochastic interpolation method [21,22]. Shokry and coworkers proposed a machine learning-based methodology for a multiparametric solution of chemical process operations [23]. This methodology has a high prediction accuracy and the complexity of the optimization solution is significantly reduced in chemical process operations. Therefore, surrogate models based on experimental data with clear trends for manipulated variables can effectively predict data in ranges for which the experiment was not performed.

In this study, processes converting shale gas to aromatics and H_2 with non-oxidative and CO_2 co-feeding reactions are optimized to reduce the BTX production cost without additional processes to utilize CH_4. The reactor performance for non-oxidative and CO_2 co-feeding reactions is designed as a surrogate model using GPR, and experimental data for the corresponding operating conditions, including the CO_2 concentration, temperature, and feed composition, are obtained. The hyperparameter of GPR is optimized using a Bayesian optimization algorithm, and the predicted results are compared with the experimental results. Based on the surrogate model, an optimizer is designed to minimize the thermal energy demand and maximize total profit of both processes. Furthermore, the CO_2 emissions and economic feasibility of the proposed BTX production processes are compared with those of commercial BTX production processes (naphtha reforming and Cyclar processes) and ECC process using shale gas. To ascertain the economic impact of CO_2 emissions on the process, the economic evaluation is performed again by applying the carbon price to the CO_2 emission of the evaluated processes.

2. Process description

2.1. Process of converting shale gas to aromatics and H_2

CH_4, C_2H_6, and C_3H_8 are major components of shale gas; CH_4 constitutes the largest proportion (85–90 %). In methane dehydroaromatization (MDA), the initial conversion of CH_4 is approximately 10–12 % at 973 K using the Mo-based ZSM-5 catalyst, and the corresponding BTX yield is approximately 5–6 % [24,25]. BTX yield in shale gas aromatization can be higher than that in MDA owing to the presence of C_2H_6 and C_3H_8. However, it is not possible to convert all of the CH_4 in shale gas. Therefore, methods for improving the yield of by-products by modifying the reaction system (CO_2 co-feeding) or for removing unreacted CH_4 in advance without altering the reaction system (non-oxidative) can be considered.

The schematic diagram of converting shale gas to aromatics and H_2 is depicted in Fig. 1. The shale gas is assumed to contain approximately 85, 10, and 5 % of CH_4, C_2H_6, and C_3H_8, respectively. For non-oxidative BTX production, shale gas is supplied to the distillation column (CL-1). The distillation column selectively separates CH_4, and the remaining gases are supplied to the heat exchanger (H-1). H-1 receives heat from the furnace and is used to increase the temperature of the feed stream to the reaction temperature. From the results of previous economic analyses [4], the processes to convert shale gas into aromatics and H_2 are not economically feasible when used independently. The process economics can be improved by introducing a process utilizing CH_4, such as H_2 and CH_3OH production. The main reasons for the increased capital costs are the BTX yield, which is lower than that of the existing BTX production process, and unreacted CH_4, which acts as an inert gas for the subsequent process. In Fig. 1, we propose partially removing CH_4 in advance using a distillation column, and supplying it to the subsequent process for non-oxidative BTX production. In contrast, in the CO_2 co-feeding BTX production process, the distillation unit is not used due to the decrease of BTX yield. These different process configurations are based on experimental data and are comprehensively described in the Results and Discussion section. For BTX production, two BTX reactors are considered: one is used for reactions (R-1) and the other for catalyst regeneration (R-2). In the non-oxidative BTX production process, BTX is produced from the modified shale gas; a membrane module (M−1) and a series of distillation columns (CL-2 and 3) are needed to separate H_2, CH_4, and BTX. For the CO_2 co-feeding BTX production process, the feed gas (MX-1) is mixed with CO_2 and then supplied to the BTX reactor. In the BTX reactor, shale gas aromatization and dry reforming reactions occur simultaneously to produce BTX, H_2, and CO. In this reaction system, not only aromatization and dry reforming of HCs, but also the possibility of reverse water–gas shift (RWGS, $CO_2 + H_2 \leftrightarrow CO + H_2O$) reaction exists. If H_2O is generated during the reaction, zeolite is deactivated. However, in the H balance of experimental data, the output H/input H converges to 1 even though H_2O is not considered. This suggests that the RWGS reaction did not occur, and the formation of H_2O was excluded in advance from the analysis of our proposed process. The product stream is compressed at a high pressure using a compressor to separate the light HCs and H_2 (CP-1, 2, and 3). The product stream from the BTX reactor flows into the membrane module (M−1) for separating H_2. The CH_4–BTX–CO mixture is supplied to a series of distillation columns to separate CH_4–CO and BTX (CL-2 and 3). The separated CH_4–CO mixture is supplied to the pressure swing adsorption (PSA) unit (PSA-1) to obtain the products CO and CH_4. For the CO_2 co-feeding BTX production process, CO is produced at twice the number of moles of CO_2 input. The composition and conditions of the shale gas and the operating conditions of the process are shown in Tables 1 and 2, respectively.

In Table 2, most of the parameters are fixed; however, the CH_4 recovery rate of the CH_4 distillation column, reaction temperature during BTX production, and amount of CO_2 supply are variables. All these variables must be optimized because they are critical factors that determine the economic feasibility for the conversion of shale gas to aromatics and H_2, as determined in a previous study [4].

2.2. Gaussian process regression (GPR)

The proposed BTX production from shale gas involves various reactant and product components. In addition, a markedly different trend is

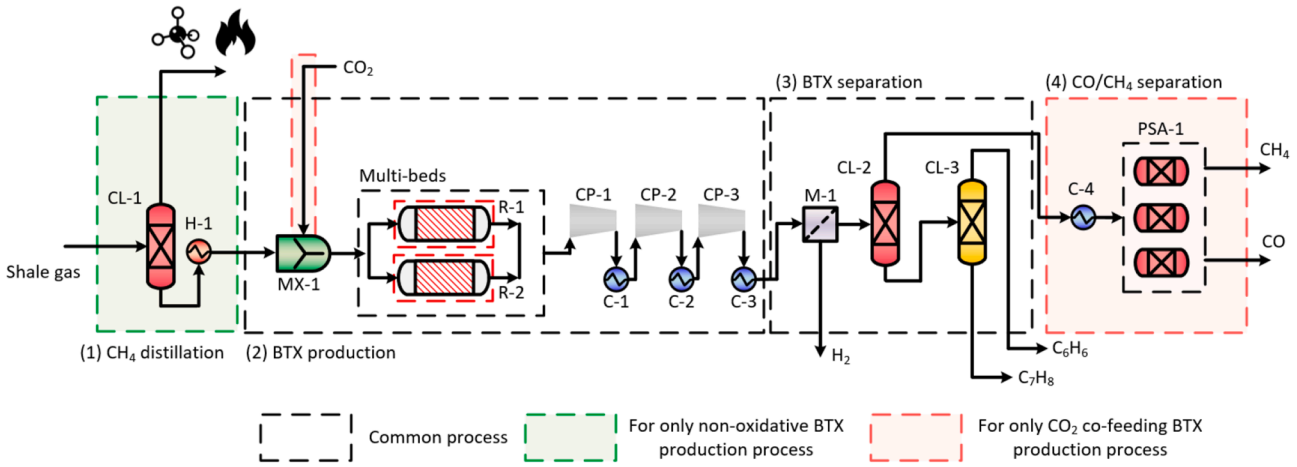

Fig. 1. Schematic diagram for converting shale gas to aromatics and H_2; non-oxidative BTX production integrated with a methanizer and CO_2 co-feeding BTX production integrated with CO/CH_4 PSA. CL: column, H: heater, C: cooler, MX: mixer, R: reactor, CP: compressor, M: membrane module, and PSA: pressure swing adsorption.

Table 1
Shale gas composition and conditions used in this study.

Composition	Value (mol%)	Condition	Value
CH_4	85	Temperature	313 K
C_2H_6	10	Pressure	30 bar
C_3H_8	5	Flow rate	90,000 kg/h

Table 2
Operating conditions for CH_4 distillation, BTX production and separation, and PSA unit.

	CH_4 distillation
Pressure	30 bar
CH_4 recovery rate	Variables
	BTX production
Pressure	1 bar
Temperature	Variables
CO_2 concentration	Variables
Catalyst	Mo/HZSM-5
Compression ratio	2.34
	BTX separation
Feed pressure of M−1	30 bar
Permeate pressure of M−1	1 bar
Pressure of CL-2	30 bar
Pressure of CL-3	1 bar
	PSA unit
Pressure	30 bar
Temperature	313 K
Sorbent	Cu-based activated carbon [26]

observed depending on the reaction temperature and the presence or absence of CO_2 in the feed stream. Information on this reaction is typically elucidated through fundamental kinetic studies based on the type of metal and the mechanism of the acidic site of zeolite [27]. However, the overall performance of the process is greatly affected by the product distribution of the reactor. That is, it is enough to obtain reactor output according to feed composition or operating conditions. Accordingly, an approach using a surrogate model such as GPR may be more efficient than that using kinetic modeling with a large computational load and strong uncertainty (Fig. 2). We used the Mo/HZSM-5 catalyst to obtain BTX yield and yields of all other components for various CO_2 concentrations, reaction temperatures, and shale compositions. These data indicate a clear trend for manipulated variables; therefore, it is an appropriate dataset for using GPR. GPR models are nonparametric kernel-based probabilistic models that have been extensively used in machine learning applications owing to their representation flexibility and inherent uncertainty measures over predictions. In general, GPR models are represented as follows [28]:

$$f(x) \sim GP(m(x), K(x, x^{'})) \tag{1}$$

where x, $f(x)$, $m(x)$, and $K(x,x')$ denote the training input, and objective, mean, and covariance functions, respectively. In this study, a covariance function was obtained using the Matérn 3/2 kernel function, which is represented as follows [29]:

$$K(x, x^{'}) = \theta_0 \left(1 + \sqrt{3r^2(x, x^{'})}\right) \exp\left(-\sqrt{3r^2(x, x^{'})}\right) \tag{2}$$

where θ_0 and $r^2(x,x')$ denote the amplitude and positive parameter of the covariance, respectively. The covariance amplitude and length scale are hyperparameters that define the behavior of the objective function.

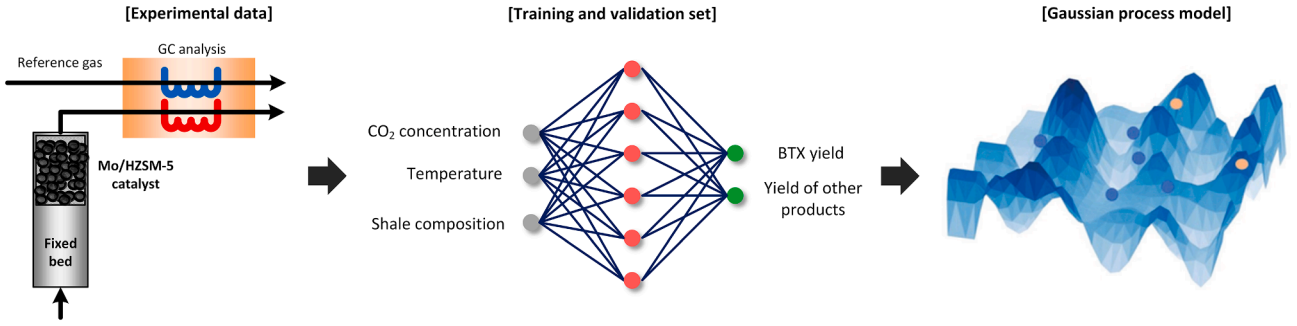

Fig. 2. Gaussian process regression (GPR) model using the experimental data.

Bayesian optimization is used to optimize these hyperparameters [30]. Three different process parameters, namely, CO_2 concentration, temperature, and composition, are identified as input variables in the GPR model; the output variables includes the BTX yield, CH_4 conversion rate, and H_2 production ratio (mol-H_2/mol-C). GPR based on Bayesian optimization is a widely used algorithm, and detailed descriptions are provided in Supporting Information.

3. Experimental section

A 10 wt% Mo/HZSM-5 catalyst used in this study was prepared using commercial HZSM-5 and ammonium molybdate tetrahydrate ($(NH_4)_6Mo_7O_{24}$–$4H_2O$). The detailed synthesis procedure is described in our previous study; additionally, the characteristics of the catalyst are presented [4]. The BTX yield, CH_4 conversion, and H_2 production ratio of non-oxidative and CO_2 co-feeding BTX production when $CH_4/C_2H_6/C_3H_8$ = 85/10/5% are specified in the Supporting Information. In this section, only the experiments on the composition of CH_4 are considered.

Table 3 lists the experimental conditions for four different sets of the feed. A laboratory experimental fixed-bed reactor was set up; the diameter of the fixed-bed reactor and packed height of the catalyst were 0.009 and 0.02 m, respectively, and approximately 0.2 g catalyst was used. The carburization was initiated after the temperature of the catalyst in the bed increased to 923 K, and a mixture of N_2/CH_4 (N_2:CH_4 = 1:1) was used. During carburization, the N_2/CH_4 mixture was supplied at a flowrate of 6.0 L/g-cat•h for 0.5 h. Immediately after the carburization, the reactor was heated to the reaction temperatures list in Table 3. The reactor was operated at atmospheric pressure, and the total gas hourly space velocity (GHSV) was maintained at 3.0 L/g-cat•h during the reaction. In Sets 1 and 2, CO_2 was not supplied, and only the $CH_4/C_2H_6/C_3H_8$ mixture was used. The difference between Sets 1 and 2 is the composition of CH_4. In Sets 3 and 4, 10 % CO_2 was added to the same shale gas compositions considered in Sets 1 and 2, respectively. The compositions of all products were analyzed using gas chromatography.

4. Results and discussion

4.1. BTX yield according to the CH_4 composition variation

The BTX formation rates of Sets 1 and 2 under the non-oxidative BTX production process are shown in Fig. 3**a**. The thermodynamic limitation is estimated using the Gibbs energy minimization method, assuming that coke and naphthalene are not produced [31]. In other words, it represents the maximum BTX formation rate under ideal conditions. The thermodynamic limitations of Set 1 with 85 % CH_4 and Set 2 with 5 % CH_4 are markedly different. This reflects that the probability of CH_4 changing to BTX in Set 2 is lower than in Set 1. In experiments with significantly different moles of C in the feed gas (Sets 1 and 2), the BTX formation rate is almost similar while the catalyst activity is maintained. The activity of CH_4 under Mo_2C is evident [32,33], which implies that the BTX yield can be reduced when the CH_4 content in the shale gas is zero. Additionally, this study confirms that the case with only 5 % CH_4 has almost the same BTX formation rate as that of the existing shale gas composition, suggesting that the capacity of the downstream process can be reduced by controlling the amount of CH_4 in the feedstock. The experimental BTX formation rate is approximately 75 % of the thermodynamic limitation in Set 2 and approximately 49 % in Set 1. This indicates that a substantial amount of CH_4 in shale gas cannot be converted to BTX for current catalytic reaction system. Based on the experimental results, the conversion of CH_4 to BTX is more challenging than that of C_2H_6/C_3H_8 to BTX.

Table 3
Experimental feed conditions.

	Set 1	Set 2	Set 3	Set 4
	Non-oxidative		CO_2 co-feeding	
Total gas flow rate	3.0 L/g-cat•h			
Reactant gas flow rate	1.5 L/g-cat•h			
$N_2/CH_4/C_2H_6/C_3H_8$ (%)	0/85/10/5	80/5/10/5	0/85/10/5	80/5/10/5
Balance-gas flow rate	1.5 L/g-cat•h			
N_2 concentration (%)	100	100	90	90
CO_2 concentration (%)	0	0	10	10
Temperature	973 K		1023 K	
Pressure	1 bar			

When CO_2 is co-fed into BTX reactor with shale gas, the trend is completely different from that in the absence of CO_2, as shown in Fig. 3**b**. When the composition of CH_4 is low (Set 4), the BTX formation rate is approximately 37.5 % lower than that for the high composition (Set 3). As CO_2 is supplied, the thermodynamic limitation for the same composition (Set 1 and Set 3/Set 2 and Set 4) is significantly reduced. Owing to the addition of CO_2, the BTX formation rate is reduced. The reduction in the thermodynamic limitation depends on the composition of CH_4, which indicates that reducing CO_2 to CO is more thermodynamically favorable than aromatizing HCs. In Set 3, the BTX formation rate is approximately 53 % of the thermodynamic limitation. In Set 4, except for the initial induction period, the rate approaches the thermodynamic limitation. Specifically, compared with Set 2 (Fig. 3**a**), almost all HCs are converted to BTX, except dry reforming of HCs while CO_2 is co-fed in Set 4.

Fig. 3 indicates that the installation of a distillation unit for CH_4 separation in the process of converting shale gas to BTX, similar to that used in the ECC, depends on the presence of CO_2 in the reactant. By removing a significant amount of CH_4 in advance using a distillation unit under non-oxidative conditions, the volume of the subsequent processes can be considerably reduced. However, if the distillation unit is used under conditions in which CO_2 is co-fed, severe BTX formation loss occurs, which negatively affects the process economics.

4.2. Experimental data based surrogate model validation

Fig. 4 shows the surrogate model validation for BTX yield, CH_4 conversion rate, and H_2 production ratio. Bayesian optimization was applied to all three targets. The optimized hyperparameters are listed in Table 4. The results of the Matérn 3/2 kernel function compared with those of other kernel functions are listed in **Table S2**. In addition, it should be noted that the surrogate model used in this study was constructed based on 10 wt% Mo/ZSM-5 catalyst and the limited operating conditions. This surrogate model can cover the temperature of 973–1073 K and CO_2 concentration of 0–20 % at fixed GHSV of 3 L/g-cat.·h. The Gaussian Process (GP) estimates of the BTX yield, CH_4 conversion rate, and H_2 production ratio are shown in Fig. 4**a** in terms of the training set, prediction data, GP function, and 95 % prediction intervals. The confidence intervals for the BTX yield and CH_4 conversion rate appear slightly wide, whereas the H_2 production ratio has a narrow confidence interval. Despite the wide confidence intervals of the BTX yield and CH_4 conversion rate, the GP function appears to be sufficiently consistent with the experimental data. The parity curves of the training and validation sets for BTX yield, CH_4 conversion rate, and H_2 production ratio are shown in Fig. 4**b**, where 90 % of all experimental data are randomly sampled for the training set and the remaining 10 % for the validation set (Table 4). Similar to Fig. 4**a**, the H_2 production ratio exhibits the highest fitting performance, followed by the BTX yield and CH_4 conversion rate; an error within 6 % is validated. Fig. 4**c** depicts the output of the surrogate model based on the CO_2 concentration and reaction temperature. The peak of the BTX yield appears at a CO_2 concentration of approximately 7.5 % and a reaction temperature of approximately 1023 K. Since the amount of CH_4 generated by cracking of C_2H_6 and C_3H_8 during the reaction is greater than the amount of converted CH_4, the apparent CH_4 conversion rate is negative. Compared with other conditions, the CH_4 conversion rate presents a generally low value when the concentration of CO_2 is 0 % and especially at

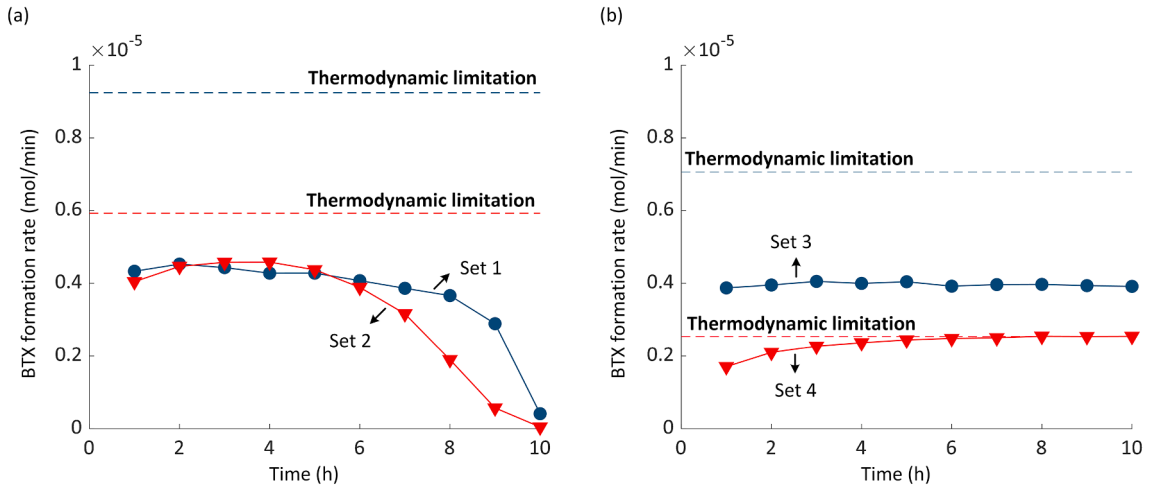

Fig. 3. BTX formation rate according to the change in CH_4 concentration: (a) non-oxidative and (b) CO_2 co-feeding BTX production; Thermodynamic limitations of various feed conditions are estimated from the Gibbs free energy minimization method, using the Peng–Robinson equation of state to calculate the required fugacity coefficients.

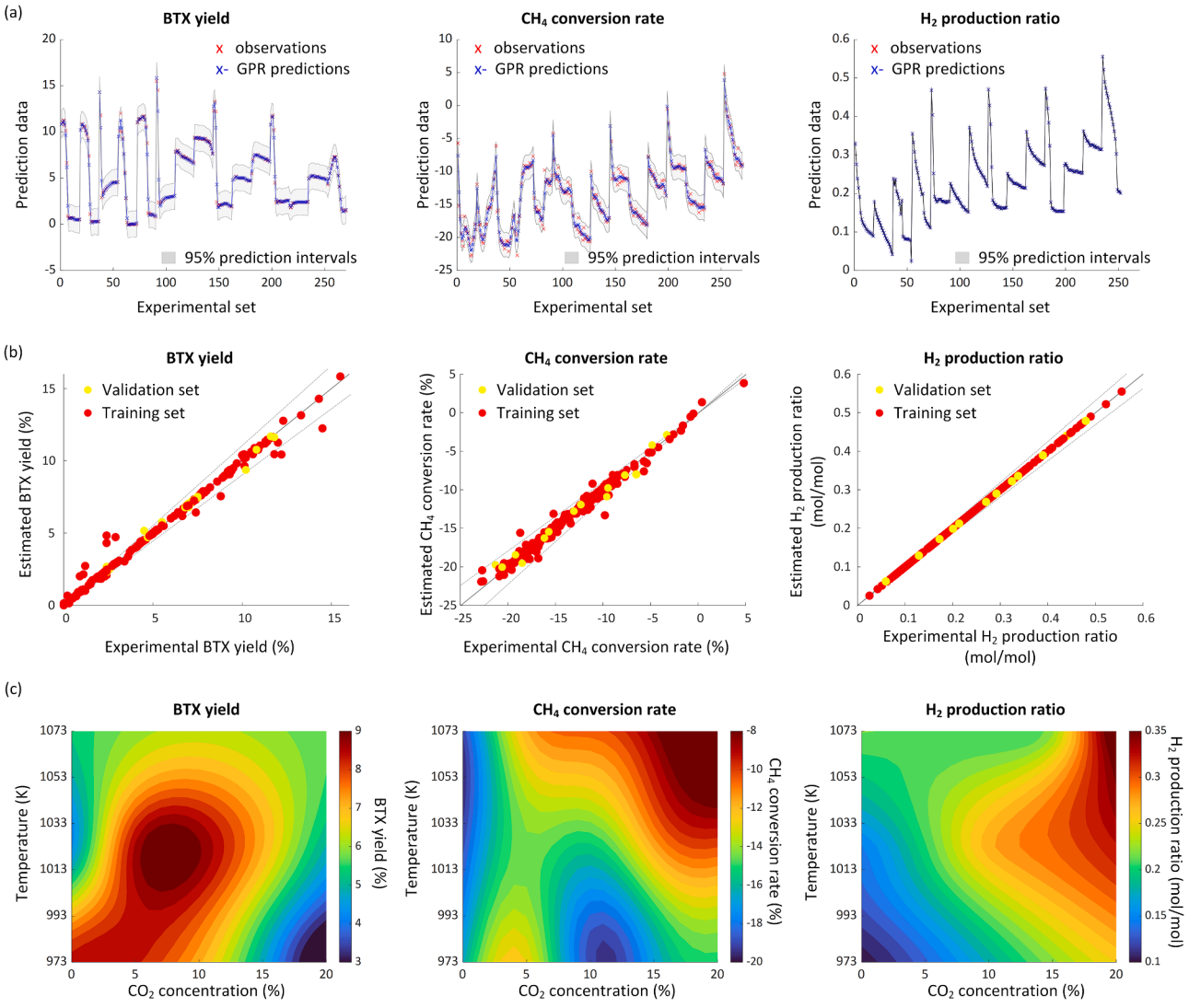

Fig. 4. Surrogate model validation for BTX yield, CH_4 conversion rate, and H_2 production ratio (mol-H_2/mol-C in feed): (a) GP estimates, (b) parity curves of experimental and predicted data in training and validation sets, and (c) optimized GPR model according to the CO_2 concentration and reaction temperature; All data are listed in **Table S1** in Supporting Information.

Table 4
Hyperparameter optimization.

	BTX yield	CH_4 conversion rate	H_2 production ratio
No. of training samples	243	243	225
No. of validation samples	27	27	27
Sigma	14.5883	0.0001069	0.0001027
Kernel length scale	0.5172	0.1053	1.6225
RMSE	1.1892	1.2179	0.0142

concentrations in the range of 10–15 % and temperatures below 1013 K. In this region, C_2H_6 and C_3H_8 are not converted to olefins and have high selectivity for BTX and CH_4. Moreover, the BTX yield is predominantly maintained in this range. The H_2 production ratio generally increases as the concentration of CO_2 and the reaction temperature increase.

4.3. Optimization and process simulation

Fig. 5 shows the optimization results based on the GPR model for the non-oxidative and CO_2 co-feeding BTX production processes. The operation time of the reactor is set at the point in time when the BTX yield decreases by 1 % or more in absolute value compared to the initial BTX yield. That is, the operation time is set according to the stability of the reaction, as shown in Fig. 5**a**. The operation time is significantly increased with increasing CO_2 concentration. However, at temperatures approaching 1033–1073 K, the operation time is decreased regardless of the CO_2 concentration. Fig. 5**a** indicates that the CO_2 concentration must be increased to more than 10 % to obtain the long operation time (greater than 10 h) of the reactor. Moreover, the process should not be operated at temperatures exceeding 1033 K. The maximum operation times for non-oxidative and CO_2 co-feeding BTX production are 7 and 18 h, respectively. Accordingly, the reactor enthalpy change in terms of the reaction temperature and CO_2 concentration is shown in Fig. 5**b**. In the ranges of 0–10 % CO_2 and 973–1033 K, the reactor enthalpy change has lower values than those in other conditions (200–300 kJ/mol-BTX). This range is derived as a combination of the reaction enthalpies of the aromatization, dry reforming, and exothermic cracking reactions. The enthalpy significantly changes with the increasing concentration of CO_2, leading to the decreases for the productivity of BTX, while substantial amounts of H_2 and CO are generated by dry reforming. For the same concentration of CO_2, the reactor enthalpy sharply changes above 1033 K, which can be attributed to instantaneous H_2 generation owing to the short reaction time in Fig. 5**a**. The BTX reactor with non-oxidative and CO_2 co-feeding produces H_2 and CO in addition to BTX. The mass flow rates of all the products are shown in Fig. 5**c** ($CH_4/C_2H_6/C_3H_8 = 85/10/5$%, 100 kmol/h). Above 1033 K, the operation time is short; consequently, BTX and H_2 are generated to the maximum extent, and the highest total productivity is observed. As the CO_2 concentration increased above 10 %, the yield of BTX is significantly decreased, thus decreasing the total production rate. The thermal energy demand of the proposed process must be determined for R-1, R-2, CL-1, CL-2, and CL-3, as shown in Fig. 1. For non-oxidative BTX production, the optimal thermal energy demand is investigated at a reaction temperature of 993 K. At a low reaction temperature, the BTX yield is low; thus, the thermal energy demand in R-1 and R-2 is reduced. In addition, the reboiler duty is reduced in CL-1 and CL-2. As the reaction temperature is increased, the thermal energy demand increases due to the reaction heat required for the BTX formation reaction and the increasing reboiler duty of CL-1 and CL-2. In the production of BTX with CO_2 co-feeding, the optimum

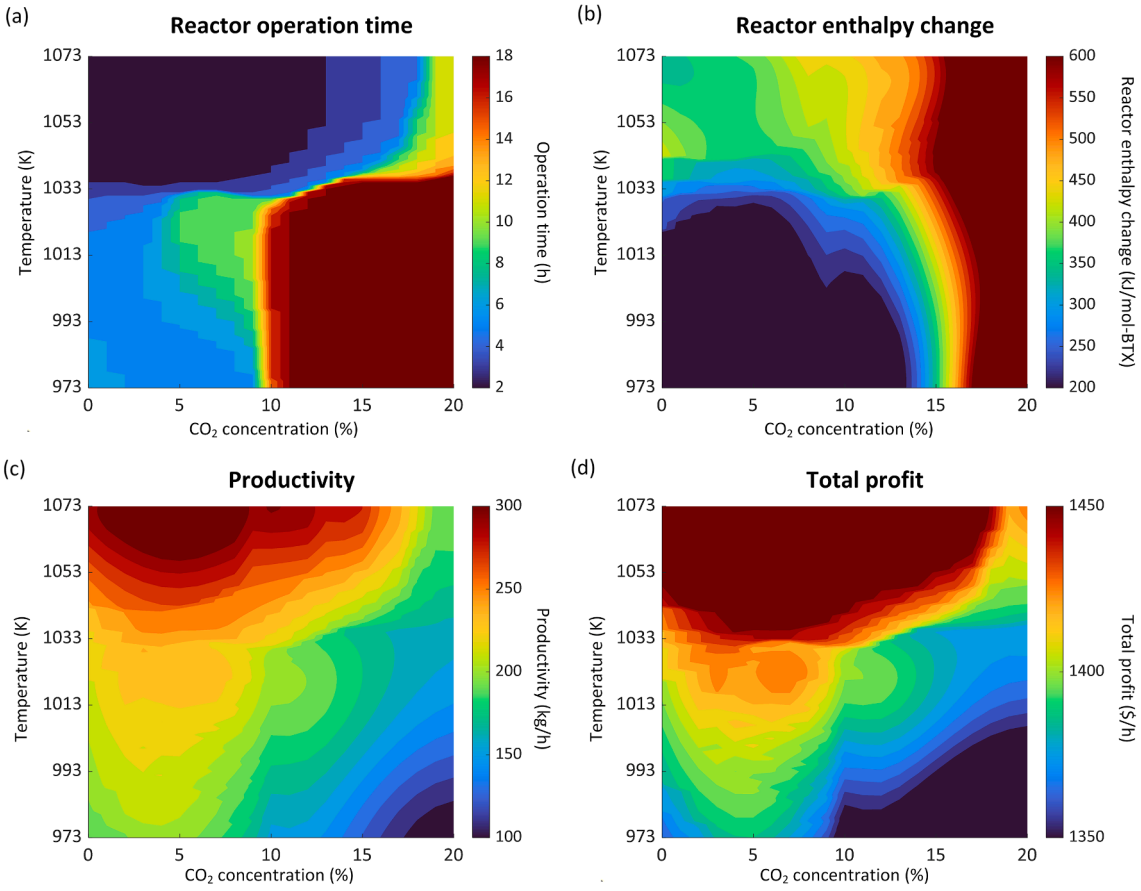

Fig. 5. Optimization results: (a) reactor operation time, (b) reactor enthalpy change, (c) productivity, and (d) total profit, including that of BTX, CO, and H_2, as a function of the reaction temperature and CO_2 concentration.

point for thermal energy demand is confirmed for a CO_2 concentration of 10.6 % and reaction temperature of 1027 K. As the CO_2 concentration is increased, the demand for thermal energy consumed in R-1 (reaction) increases owing to the combination of endothermic heat by dry reforming and aromatization. However, the thermal energy demand consumed in R-2 (regeneration) is decreased because the amount of coke decreases with increasing CO_2 concentration. In addition, the reboiler duty for CL-2 simultaneously increases with the increasing CO_2 concentration. In contrast, in CL-3, the BTX yield decreases with increasing CO_2 concentration, thus reducing the reboiler duty. In our previous study, the thermal energy demand accounted for 63 % (except feedstock) of the total chemical production cost for both non-oxidative and CO_2 co-feeding BTX production. Therefore, the optimization of the total thermal energy demand implies that the total production cost is minimized.

The total profit, including that of BTX, H_2, and CO, is shown in Fig. 5**d**; it shows a trend similar to that of productivity. As the concentration of CO_2 increases, the profit appears to temporarily increase owing to the increase in the concentration of H_2. However, the total profit decreases owing to a considerable decrease in the BTX output. On the basis of the evaluation platform for the proposed BTX production (**Fig. S1**), the optimized operating condition obtained by combining all the profiles in Fig. 5 is a reaction temperature of 1013 K for non-oxidative BTX production. For CO_2 co-feeding BTX production, the concentration of CO_2 is 10.5 %, and the reaction temperature is 1025 K. For the non-oxidative and CO_2 co-feeding BTX production, modeling is performed considering the abovementioned optimized conditions. The comparative ECC, naphtha reforming, and Cyclar processes are simulated by referring to commercial process designs. The modeling and simulation results are summarized in Supporting Information (**Figs. S2–S5** and **Tables S3–S7**). We adopted a co-cracking design (C_2H_6/C_3H_8) for the ECC process, general naphtha reforming design, and Cyclar process using a C_3H_6/C_4H_8 mixture (50/50 wt%).

4.4. Life cycle assessment (LCA)

The framework of the LCA methodology is represented in the literature according to the International Standards Organization [34]. In this study, the environmental impact was analyzed by performing the LCA of two BTX production processes from shale gas and ECC with the same feedstock. The final product of ECC is ethylene, which is different from the proposed BTX processes. The downstream processes of these products (*i.e.*, product use and disposal phase) were not included in the LCA boundary, and only the environmental impact of the chemical production process was estimated. Consequently, the gate-to-gate boundary was adopted instead of the cradle-to-grave system boundary since the upstream processes for extracting shale gas were identical in both schemes [35]. The major product of naphtha reforming and Cyclar processes are same as the BTX production process proposed in this study. However, since the feedstock of above processes is different, and byproducts other than BTX are generated. In the sense of comparing the environmental impact from the input of raw materials to the production of BTX with different processes, the gate-to-gate boundary is effective.

Most importantly, the global warming impacts (GWIs) of the proposed non-oxidative and CO_2 co-feeding BTX production process are compared with those of ECC, naphtha reforming, and Cyclar processes. GWI is a single, convenient global warming metric calculated as accumulated greenhouse gas (GHG) emissions and expressed as CO_2 equivalents (CO_2 eq) by weighting the global warming potential [35]. Electricity, steam, and direct CO_2 emissions are the main factors that influence GWI. The platform for the gate-to-gate LCA is shown in **Fig. S6**, and the ecoinvent database summary used in this study is listed in **Table S8**. All databases refer to the openLCA ecoinvent database and CO_2 emission factors [36], and the CML method is used for the LCA (**Table S9**). For all evaluated processes, direct CO_2 emissions from the process/coke removal and indirect CO_2 emissions from steam/electricity are estimated.

Fig. 6**a** shows a schematic of the CO_2 emission evaluation for BTX production using CO_2 co-feeding. In contrast to the other processes, CO_2 is added to the feed. The total CO_2 emission is the sum of CO_2 emitted when producing chemicals, the energy demand consumed for separation, and direct emissions. Additionally, CO_2 is reduced and treated as a CO product; therefore, the CO_2 emissions may be decreased. In this study, it is assumed that 277 kWh/t-CO_2, the energy demand of the post-combustion CO_2 capture process [37], was used to supply CO_2, and it is necessary to note that it was applied to the above LCA. The LCA results for non-oxidative BTX production, CO_2 co-feeding BTX production, and ECC are shown in Fig. 6**b**. All factors are normalized using the environmental impacts of ECC process designed in this study; the normalized factors are listed in **Table S11**. As shown in Fig. 6**b**, the environmental impact of ECC process is set to 1, and the relative magnitudes of the non-oxidative and CO_2 co-feeding BTX production processes are represented. In ECC, the environmental impacts are lower than those of non-oxidative BTX production owing to the relatively low demand for utilities. However, for the CO_2 co-feeding BTX production process, all environmental impacts are considerably lower than those of the conventional ECC process.

Among the environmental impacts, CO_2 emissions from CO_2 co-feeding BTX production are significantly lower than those from the other processes. The detailed breakdown of CO_2 emissions from non-oxidative BTX production, CO_2 co-feeding BTX production, ECC, naphtha reforming, and the Cyclar process is shown in Fig. 6**c**. This includes both direct CO_2 emissions from the process and indirect CO_2 emissions using electricity and steam. The CO_2 emissions from the ECC are estimated to be 1.91 kg-CO_2 eq/t-ethylene, and the reference range is 1.39–2.13 kg-CO_2 eq/t-ethylene [38]. The Cyclar process and naphtha reforming demonstrate values of 0.79 and 0.99 kg-CO_2 eq/t-(BTX + H_2), respectively. The energy distribution of the naphtha reforming process modeled in this study is well designed, as it is equivalent to approximately 0.99 kg-CO_2 eq/t-BTX in the reference plant [39]. The non-oxidative BTX production in the present study results in approximately 1.52 kg-CO_2 eq/t-(BTX + H_2), and the proportion of indirect emissions is considerably higher than that of direct emissions. In the CO_2 co-feeding BTX production process, despite using the same feed as that in the non-oxidative process, 0.33 kg-CO_2 eq/t-(BTX + H_2 + CO) is obtained. Furthermore, CO_2 supplied to the reactor is reduced to the product CO, leading to the decrease of total CO_2 emissions within the LCA boundary. According to our previous study [7], the CO_2 emissions are not decreased unless a carbon-containing product is obtained from co-fed CO_2. In the CO_2 co-feeding process, CO from the BTX reactor is separated from CH_4 and treated as a product, thus providing the possibility of reducing CO_2 emissions.

4.5. Technoeconomic analysis (TEA)

Technoeconomic analysis (TEA) was performed to determine the economic feasibility of the proposed BTX production method by comparing it with that of conventional processes and determining the levelized cost of BTX production (LCB), including income taxes and capital investment/depreciation. The economic analysis for the processes can be classified into capital expenditure (CAPEX; including equipment purchase and installation and construction costs) and operating expenditure (OPEX; mainly including the operation and maintenance costs). Calculations for the ECC, Cyclar, and naphtha cracking processes are detailed in Supporting Information.

From the optimized conditions and heat and material balances calculated using Aspen Plus V10, the sizes and costs of all the units in Fig. 1 are estimated using the Aspen Process Economic Analyzer V10. The CAPEX process equipment, supporting facilities, and direct and indirect labor estimations of the overall process are conveniently calculated using empirical correlations [40] and data from reference plants [41,42]. In particular, the BTX-reactor CAPEX including the catalyst

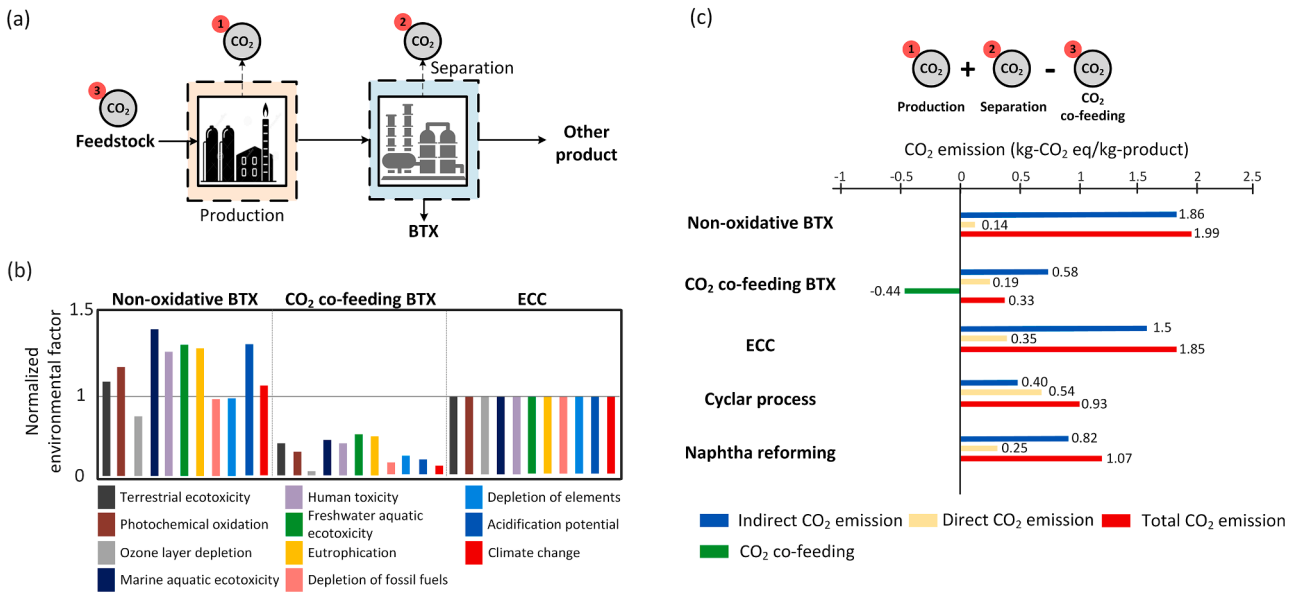

Fig. 6. Life cycle assessment results: (a) schematic of CO_2 emission evaluation; (b) environmental impacts of non-oxidative BTX production, CO_2 co-feeding BTX production, and ethane cracking center (ECC); (c) CO_2 emissions including direct and indirect emissions. **Table S10** presents the analysis of environmental influences.

prices, which are high during BTX production, is based on actual industrial plant data and calculated using the exponential scaling expression described in the National Renewable Energy Laboratory (NREL) report [43]. In addition, the cost of replacing a completely deactivated catalyst, as presented in the NREL report, is included in OPEX. The replacement cycle for the Mo/HZSM-5 catalyst is set to 6 months, which is relatively shorter than that of Ga/HZSM-5 catalysts in Cyclar process. Furthermore, the CO_2 supply cost is set at approximately 60 \$/t-CO_2 based on an absorption-based CO_2 capture process using a 30 wt% solution of monoethanolamine [44]. Based on our detailed summary of previous economic analyses, we apply cash flow analysis based on the net present value (NPV). The LCB was defined at NPV = 0.

$$\text{Net earnings (NE)} = (\text{Sales} - C_{Exel.Dep.} - C_D) \times (1.0 - t_{income}) \tag{3}$$

$$\text{Annual cash flow (CF)} = (\text{NE} + C_D) - C_{\text{TDI}} \tag{4}$$

$$\text{NPV} = \sum_{n=1}^{N_{life}} \frac{\text{CF}_n}{(1+i)^n} \tag{5}$$

$$\text{NPV (LCB)} = 0 \tag{6}$$

where $C_{\text{Excel.Dep.}}$ [MM\$/year], C_D [MM\$/year], t_{income} [MM\$/year], C_{TDI} [MM\$/year], and N_{life} [year] represent the production costs exclusive of depreciation, depreciation, tax income, total capital investment, and plant life, respectively. Our economic evaluation considers the assumptions and parameters listed in Table S12–S13.

In the 2015 Paris Climate Agreement, countries agreed to retain the increase in global average temperature well below 2 °C above pre-

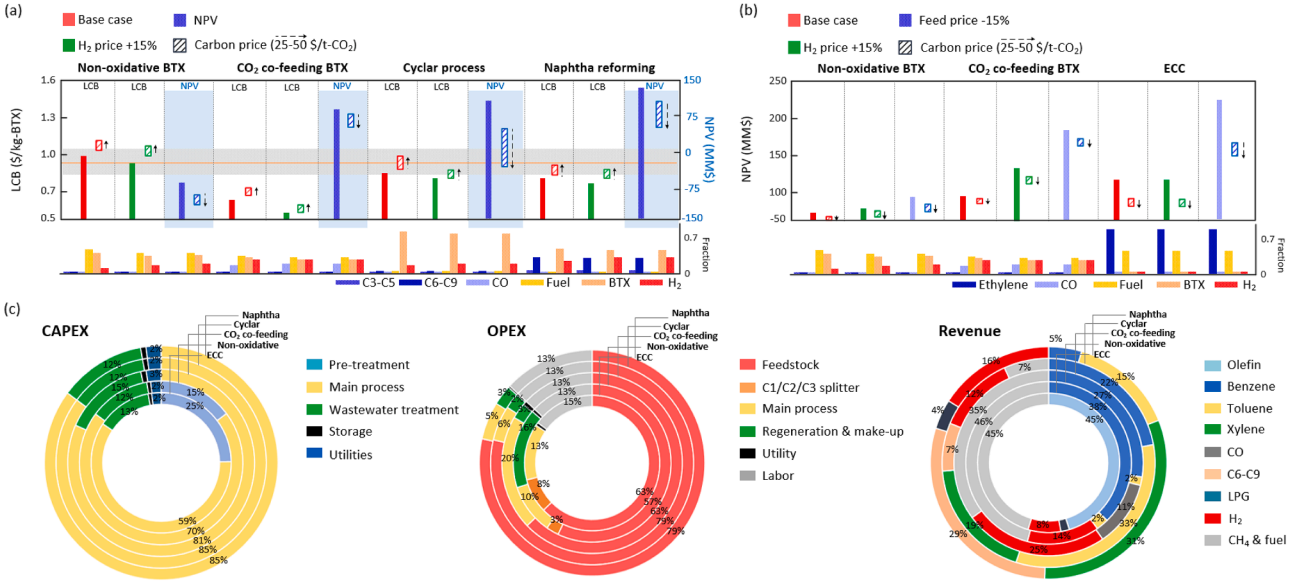

Fig. 7. TEA results: (a) LCB and sensitivity analysis for non-oxidative and CO_2 co-feeding BTX production, Cyclar, and naphtha reforming processes; (b) NPV and sensitivity analysis for the non-oxidative and CO_2 co-feeding BTX production, and ECC; (c) capital and operating expenditure and revenue breakdown. Detailed TEA results are listed in **Table S14**. **Table S15** lists the detailed carbon-price based TEA results.

industrial levels and to endeavor to further limit this value to 1.5 °C [45]. Recently, by announcing policies related to carbon neutrality worldwide, a "net-zero" scenario, wherein GHG emissions are equal to zero, has been considered [46]. As with current commercial processes, we performed TEA for the two proposed BTX production processes without considering CO_2 emissions. Furthermore, the TEA was performed again by considering the current carbon price range (greater than 25$/t-$CO_2$) for commercial and developed processes.

TEA results for the optimized process of converting shale gas to aromatics and H_2 are represented in Fig. 7 with Cyclar process, naphtha reforming, and ECC. Fig. 7**a** shows the LCB with reference to non-oxidative and CO_2 co-feeding BTX production compared with those of the conventional BTX production processes. The LCB of non-oxidative BTX production is evaluated as 1.0 $/t-BTX at an optimum temperature of 1013 K. The LCB of CO_2 co-feeding BTX production at optimum operating conditions is estimated to be 0.65 $/t-BTX. These values are lower than the BTX market price of 0.82–1.05 $/t-BTX. Furthermore, for the naphtha reforming and Cyclar processes, the LCB is calculated below the market price; however, the values are higher than that of the CO_2 co-feeding process. Therefore, CO_2 co-feeding BTX production is most advantageous in terms of the production cost of BTX because the product distribution is different from that in the other processes. The bottom portion of Fig. 7**a** displays the sales distribution of the product. For the naphtha reforming and Cyclar processes, BTX and C6–C9 sales account for approximately 80 and 81 % of total product sales, respectively; they occupy the highest proportion of the total sales. However, in non-oxidative and CO_2 co-feeding BTX production processes, BTX sales account for a low proportion of the total product sales at 40 and 29 %, respectively. When the price of H_2 increases, the LCB reductions of the two proposed processes producing BTX from shale gas are higher than those of the other commercial BTX processes. From the LCB sensitivity for H_2 prices, the LCB with reference to the CO_2 co-feeding BTX production can be lower than the BTX market prices when H_2 prices are increased by 15 %. In contrast, for the non-oxidative BTX production, the H_2 production rate is lower than that of the CO_2 co-feeding process; thus the LCB is higher than the market prices. Despite this low production cost, the non-oxidative and CO_2 co-feeding BTX production processes exhibit lower economic benefits than those of the Cyclar and naphtha reforming processes from the perspective of the NPV, assuming the current market price of BTX. In the base case, the NPVs of the non-oxidative, CO_2 co-feeding, Cyclar, and naphtha reforming process are approximately −48, 93, 121, and 145 MM$, respectively. Although the non-oxidative and CO_2 co-feeding BTX production process has improved NPV than before optimization, it is still impossible to secure competitiveness with commercial processes from the point of view of NPV. Additionally, Fig. 7**a** includes the TEA results applying the carbon price for CO_2 emissions. The amount of CO_2 emissions predicted in Fig. 6 is reflected in the TEA, assuming a current carbon price of 25 $/t-$CO_2$ [47]. Therefore, the increase in the LCB for the production of BTX from shale gas, which emits relatively less CO_2, is lower than that for other commercial processes. NPV of non-oxidative and CO_2 co-feeding BTX production processes is −80 and 73.3 MM$, respectively, while that of Cyclar and naphtha reforming process is 55 and 94 MM$, respectively. Considering the carbon prices, the CO_2 co-feeding BTX production process is likely to have a higher NPV than Cyclar. Furthermore, when the carbon price increases to 50 $/t-$CO_2$, the NPV of CO_2 co-feeding BTX production (53.5 MM$) is higher than that of naphtha reforming process (45 MM$).

Fig. 7**b** compares the two developed BTX production processes in terms of NPV with that of ECC using shale gas. Owing to the high carbon yield of ECC (73 %) and the advantage of not using a catalyst, these two processes are less economical than the ECC process. However, similar to the sensitivity analysis in Fig. 7**a**, the increase in H_2 price and the decrease in shale gas price are more sensitive in the proposed process. Considering the CO_2 emissions, this suggests that the NPV of the CO_2 co-feeding BTX production is comparable to that of ECC. Finally, if the value of the carbon price increases to 50 $/t-$CO_2$, the CO_2 co-feeding BTX production becomes more economically feasible than the ECC process (26 MM$).

Fig. 7**c** shows the CAPEX, OPEX, and revenue breakdown for the proposed non-oxidative and CO_2 co-feeding BTX production compared with the conventional ECC, naphtha reforming, and Cyclar processes. The OPEX, CAPEX, and revenue of the ECC process are evaluated at the point where the levelized cost of ethylene production becomes zero. In ECC, the CAPEX of the pretreatment process accounts for approximately 25 % of the total, and the main process constitutes 59 % of the CAPEX. For the non-oxidative BTX production, the pretreatment and main processes account for approximately 15 and 70 % of the CAPEX, respectively. The pre-treatment in these two processes consists of a distillation unit of similar size. The main processes of the CO_2 co-feeding, Cyclar, and naphtha reforming processes account for 81, 85, and 85 % of the total CAPEX, respectively. In terms of the OPEX, the feedstock constitutes the largest fraction, and the feedstock of ECC, non-oxidative, CO_2 co-feeding, Cyclar, and naphtha reforming processes account for approximately 63, 57, 63, 79, and 79 %, respectively. In the ECC, the OPEX in the main process is only 13 % of the total OPEX. In the proposed non-oxidative and CO_2 co-feeding BTX production processes, the OPEX of the main process is 23–26 %, including regeneration and catalyst make-up costs. Cyclar and naphtha reforming processes have a high feedstock ratio; therefore, the OPEX in the main process is low. In this economic evaluation, the revenue distributions of the proposed non-oxidative and CO_2 co-feeding BTX production processes are noteworthy. For the ECC, olefin and CH_4 sales account for more than 90 % of the revenue. In the non-oxidative and CO_2 co-feeding BTX production processes, the sales of CH_4 are higher than those of BTX; however H_2 sales in the proposed processes are higher than those in the ECC. In particular, in the CO_2 co-feeding BTX production, the sales proportion of CO accounts for approximately 11 %. For the Cyclar and naphtha reforming processes, BTX and H_2, in addition to by-products such as C6–C9 and LPG, are included in the revenue and comprise a sufficiently large fraction.

The TEA results reveal that H_2 and CO products, as well as BTX, economically improve the proposed CO_2 co-feeding BTX production process. The BTX yield of the CO_2 co-feeding BTX production process is approximately 9.5 %; however, the total product sales, including H_2 and CO, are comparable to those of ECC and two conventional BTX production processes. In addition, the carbon prices for CO_2 emissions negatively affects the process economics of all the evaluated processes. Only the CO_2 co-feeding process demonstrates the lowest carbon price effect corresponding to the CO_2 emissions. This effect would be further maximized as the regulations on CO_2 emissions become stricter. In addition, the cost of supplying CO_2 in this study is assumed to be 60 $/t-$CO_2$, which can potentially be decreased to 40–50 $/t-$CO_2$ in advanced CO_2 capture processes by improving the total energy demand for CO_2 capture [48,49]. In addition to our previous study, a process evaluation targeting the base catalyst Mo/HZSM-5 was conducted in this study; if increased BTX and H_2 yields are obtained by further modifying the catalyst (in particular, in the case of non-oxidative BTX production), it is expected to be competitive with existing commercial processes. Furthermore, the regeneration stability of Mo/HZSM-5, which is considered the weakest point of this process, must be improved through catalyst development and regeneration strategies.

5. Conclusions

We optimized processes to convert shale gas to aromatics and H_2 with two different configurations (*i.e.*, non-oxidative and CO_2 co-feeding BTX production processes). The proposed process configurations were determined by experimental results based on the CH_4 content of the shale gas. In the non-oxidative BTX production process, the pre-rejection of CH_4 enhanced the BTX yield of the reactor, thereby improving the process economics. However, in the CO_2 co-feeding BTX production,

CH_4 was not pre-rejected owing to the significant reduction in the BTX yield. Based on these results, two strategies were used for producing BTX from shale gas.

The experimental data set for non-oxidative and CO_2 co-feeding BTX production was used to develop the GPR model, and hyperparameter optimization of the GPR model was performed using Bayesian optimization. From the GPR-based model, economic parameters such as thermal energy demand were optimized, and LCBs of the two proposed processes were calculated. In addition, the CO_2 emissions of the economically optimized processes were evaluated. In the non-oxidative BTX production, the CAPEX of the downstream processes was considerably decreased by installing the distillation unit, thus demonstrating improved economic feasibility. In the CO_2 co-feeding BTX production, the production of CO and H_2 indicated substantial improvement in economic feasibility.

Both processes were evaluated in terms of economy and CO_2 emissions and compared with the results of ECC, which is a shale gas-based process, and the Cyclar and naphtha reforming processes, which produce BTX. CO_2 co-feeding BTX production exhibits the lowest CO_2 emissions, and non-oxidative BTX production displays CO_2 emissions similar to those of other processes. Owing to the relatively low yields, the two BTX production processes proposed in this study demonstrate lower NPV than those of the commercial Cyclar and naphtha reforming processes. Moreover, from the perspective of NPV, the two BTX processes are less economical than ECC. However, the CO_2 co-feeding BTX production is comparable to that of the Cyclar and naphtha reforming processes; the sales of BTX and H_2 in this process are significantly higher than those in the non-oxidative BTX production. If the carbon price according to CO_2 emissions is reflected in the TEA, the CO_2 co-feeding BTX production is potentially more advantageous than the other processes.

A fundamental understanding of two strategies for producing BTX from shale gas and a methodology to overcome the limitation of BTX yield were presented. As determined from actual experiments, improving the regeneration of Mo-based catalysts is also a critical factor for realizing this process. Moreover, enhancing the BTX yield by catalyst modification significantly affects the process economics for both BTX production processes.

CRediT authorship contribution statement

Wonho Jung: Conceptualization, Methodology, Software, Validation, Formal analysis, Investigation, Resources, Writing – original draft, Writing – review & editing. **Hyeona Kim:** Validation, Investigation, Resources. **Hae Won Ryu:** Validation, Investigation, Resources. **Yong Hyun Lim:** Validation, Investigation, Resources. **Do Heui Kim:** Writing – review & editing, Supervision. **Jinwon Lee:** Writing – review & editing, Supervision.

Declaration of Competing Interest

The authors declare that they have no known competing financial interests or personal relationships that could have appeared to influence the work reported in this paper.

Data availability

No data was used for the research described in the article.

Acknowledgments

This research was supported by the C1 Gas Refinery Program through the National Research Foundation of Korea (NRF) funded by the Ministry of Science and ICT (2015M3D3A1A01064929) and (2021M3D3A1A01022109).

Appendix A. Supplementary material

Supplementary data to this article can be found online at https://doi.org/10.1016/j.enconman.2022.116480.

References

[1] Bruijnincx PC, Weckhuysen BM. Shale gas revolution: an opportunity for the production of biobased chemicals? Angew Chem Int Ed 2013;52:11980–7.
[2] Li X, Pei C, Gong J. Shale gas revolution: catalytic conversion of C1–C3 light alkanes to value-added chemicals. Chem; 2021.
[3] Schwach P, Pan X, Bao X. Direct conversion of methane to value-added chemicals over heterogeneous catalysts: challenges and prospects. Chem Rev 2017;117:8497–520.
[4] Jung W, Lee S, Kim H, Nam K, Ryu HW, Lim YH, et al. System-Level Analysis of Methanol Production from Shale Gas Integrated with Multibed-BTX Production. ACS Sustainable Chem Eng 2022;10:5998–6011.
[5] Shu Y, Ohnishi R, Ichikawa M. Pressurized dehydrocondensation of methane toward benzene and naphthalene on Mo/HZSM-5 catalyst: optimization of reaction parameters and promotion by CO_2 addition. J Catal 2002;206:134–42.
[6] Liu S, Dong Q. Unique promotion effect of CO and CO_2 on the catalytic stability for benzene and naphthalene production from methane on Mo/HZSM-5 catalysts. Chem Commun 1998:1217–8.
[7] Jung W, Lee S, Kim H, Nam K, Ryu HW, Lim YH, et al. System-Level Analysis for Continuous BTX Production from Shale Gas over Mo/HZSM-5 Catalyst: Promotion Effects of CO_2 co-feeding on Process Economics and Environment. Chem Eng J 2022;137992.
[8] He C, You F. Shale gas processing integrated with ethylene production: novel process designs, exergy analysis, and techno-economic analysis. Ind Eng Chem Res 2014;53:11442–59.
[9] Al-Douri A, Sengupta D, El-Halwagi MM. Shale gas monetization–A review of downstream processing to chemicals and fuels. J Nat Gas Sci Eng 2017;45:436–55.
[10] Wang Q, Chen X, Jha AN, Rogers H. Natural gas from shale formation–the evolution, evidences and challenges of shale gas revolution in United States. Renew Sust Energ Rev 2014;30:1–28.
[11] Song H, Meng X, Wang Z-J, Liu H, Ye J. Solar-energy-mediated methane conversion. Joule 2019;3:1606–36.
[12] Ren T, Patel M, Blok K. Olefins from conventional and heavy feedstocks: Energy use in steam cracking and alternative processes. Energy 2006;31:425–51.
[13] Froment GP, Van de Steene BO, Van Damme PS, Narayanan S, Goossens AG. Thermal cracking of ethane and ethane-propane mixtures. Ind Eng Chem Process Des Dev 1976;15:495–504.
[14] Rahimpour MR, Jafari M, Iranshahi D. Progress in catalytic naphtha reforming process: A review. Appl Energy 2013;109:79–93.
[15] P. Doolan, P. Pujado, Make aromatics from LPG, Hydrocarbon Processing;(USA) 68 (1989).
[16] Guisnet M, Gnep N, Alario F. Aromatization of short chain alkanes on zeolite catalysts. Appl Catal A 1992;89:1–30.
[17] McBride K, Sundmacher K. Overview of surrogate modeling in chemical process engineering. Chem Ing Tech 2019;91:228–39.
[18] Henao CA, Maravelias CT. Surrogate-based superstructure optimization framework. AIChE J 2011;57:1216–32.
[19] Cho S, Kim M, Lyu B, Moon I. Optimization of an explosive waste incinerator via an artificial neural network surrogate model. Chem Eng J 2021;407:126659.
[20] Yan W, Hu S, Yang Y, Gao F, Chen T. Bayesian migration of Gaussian process regression for rapid process modeling and optimization. Chem Eng J 2011;166:1095–103.
[21] Snoek J, Larochelle H, Adams RP. Practical bayesian optimization of machine learning algorithms. Advances in neural information processing systems 2012;25.
[22] Wu J, Chen X-Y, Zhang H, Xiong L-D, Lei H, Deng S-H. Hyperparameter optimization for machine learning models based on Bayesian optimization, Journal of Electronic. Science and Technology 2019;17:26–40.
[23] Shokry A, Medina-González S, Baraldi P, Zio E, Moulines E, Espuña A. A machine learning-based methodology for multi-parametric solution of chemical processes operation optimization under uncertainty. Chem Eng J 2021;425:131632.
[24] Ma S, Guo X, Zhao L, Scott S, Bao X. Recent progress in methane dehydroaromatization: From laboratory curiosities to promising technology, Journal of Energy. Chemistry 2013;22:1–20.
[25] Nam K, Ryu HW, Gim MY, Kim DH. Enhanced reactivity and stability in methane dehydro-aromatization over Mo/HZSM-5 physically mixed with NiO. Appl Catal B 2021;296:120377.
[26] Yun H, Kim YJ, Kim SB, Yoon HJ, Kwak SK, Lee KB. Preparation of copper-loaded porous carbons through hydrothermal carbonization and $ZnCl_2$ activation and their application to selective CO adsorption: Experimental and DFT calculation studies. J Hazard Mater 2022;426:127816.
[27] Bhan A, Nicholas Delgass W. Propane aromatization over HZSM-5 and Ga/HZSM-5 catalysts. Catalysis Reviews 2008;50:19–151.
[28] Rasmussen CE. Gaussian processes in machine learning. Summer school on machine learning: Springer; 2003. p. 63–71.
[29] Pandit RK, Infield D. Comparative analysis of Gaussian process power curve models based on different stationary covariance functions for the purpose of improving model accuracy. Renew Energy 2019;140:190–202.
[30] P.I. Frazier, A tutorial on Bayesian optimization, arXiv preprint arXiv:1807.02811 (2018).

[31] Shabbar S, Janajreh I. Thermodynamic equilibrium analysis of coal gasification using Gibbs energy minimization method. Energy Convers Manage 2013;65:755–63.
[32] Kosinov N, Hensen EJ. Reactivity, Selectivity, and Stability of Zeolite-Based Catalysts for Methane Dehydroaromatization. Adv Mater 2020;32:2002565.
[33] Han SJ, Kim SK, Hwang A, Kim S, Hong D-Y, Kwak G, et al. Non-oxidative dehydroaromatization of methane over Mo/H-ZSM-5 catalysts: A detailed analysis of the reaction-regeneration cycle. Appl Catal B 2019;241:305–18.
[34] I.O.f. Standardization, Environmental Management: Life Cycle Assessment; Principles and Framework, ISO, 2006.
[35] von der Assen N, Voll P, Peters M, Bardow A. Life cycle assessment of CO_2 capture and utilization: a tutorial review. Chem Soc Rev 2014;43:7982–94.
[36] Wernet G, Bauer C, Steubing B, Reinhard J, Moreno-Ruiz E, Weidema B. The ecoinvent database version 3 (part I): overview and methodology, The. Int J Life Cycle Assess 2016;21:1218–30.
[37] Jung W, Park J, Won W, Lee KS. Simulated moving bed adsorption process based on a polyethylenimine-silica sorbent for CO_2 capture with sensible heat recovery. Energy 2018;150:950–64.
[38] He C, You F. Deciphering the true life cycle environmental impacts and costs of the mega-scale shale gas-to-olefins projects in the United States. Energy Environ Sci 2016;9:820–40.
[39] Jiang J, Feng X, Yang M, Wang Y. Comparative technoeconomic analysis and life cycle assessment of aromatics production from methanol and naphtha. J Cleaner Prod 2020;277:123525.
[40] Turton R, Bailie RC, Whiting WB, Shaeiwitz JA. Analysis, synthesis and design of chemical processes. Pearson Education; 2008.
[41] Michailos S, Sanderson P, Villa Zaragoza A, McCord S, Armstrong K, Styring P, Mason F, Stokes G, Williams E, Zimmermann A. Methanol worked examples for the TEA and LCA guidelines for CO_2 Utilization. Global CO_2 Initiative; 2018.
[42] Goellner J, Kuehn N, Shah V, White III C, Woods M. Baseline analysis of crude methanol production from coal and natural gas. National Energy Technology Laboratory; 2014.
[43] R. Davis, L. Tao, E. Tan, M. Biddy, G. Beckham, C. Scarlata, J. Jacobson, K. Cafferty, J. Ross, J. Lukas, Process design and economics for the conversion of lignocellulosic biomass to hydrocarbons: dilute-acid and enzymatic deconstruction of biomass to sugars and biological conversion of sugars to hydrocarbons, National Renewable Energy Lab.(NREL), Golden, CO (United States), 2013.
[44] Rubin ES, Davison JE, Herzog HJ. The cost of CO_2 capture and storage. Int J Greenhouse Gas Control 2015;40:378–400.
[45] van Soest HL, den Elzen MG, van Vuuren DP. Net-zero emission targets for major emitting countries consistent with the Paris Agreement. Nat Commun 2021;12:1–9.
[46] Davis SJ, Lewis NS, Shaner M, Aggarwal S, Arent D, Azevedo IL, et al. Net-zero emissions energy systems. Science 2018;360.
[47] Newbery DM, Reiner DM, Ritz RA. The political economy of a carbon price floor for power generation. The Energy Journal 2019;40.
[48] Jung W, Park S, Lee KS, Jeon J-D, Lee HK, Kim J-H, et al. Rapid thermal swing adsorption process in multi-beds scale with sensible heat recovery for continuous energy-efficient CO_2 capture. Chem Eng J 2020;392:123656.
[49] Jung W, Lee M, Hwang GS, Kim E, Lee KS. Thermodynamic modeling and energy analysis of a polyamine-based water-lean solvent for CO_2 capture. Chem Eng J 2020;399:125714.